A Novel STT-MRAM Design With Electric-Field-Assisted Synthetic Anti-Ferromagnetic Free Layer

Runzi Hao, Lei Wang [iD], and Tai Min

State Key Laboratory for Mechanical Behavior of Materials, Center for Spintronics and Quantum Systems, School of Materials Science and Engineering, Xi'an Jiaotong University, Xi'an 710049, China

Spin-transfer torque magnetic random-access memory (STT-MRAM) is one of the next-generation nonvolatile memories, which has the most promising industrial prospect and has generated lots of new ideas. One of the continuous challenges in STT-MRAM development is to reduce the critical write current. Recently, one published paper reported that under a small electric bias voltage, the synthetic anti-ferromagnetic (SAF) multilayer system could be switched between an anti-ferromagnetic coupling state and a ferromagnetic coupling state. Based on this phenomenon, we propose a new type of STT-MRAM of which the critical write current can be reduced by an assisting electric-field (E-field). Micromagnetic simulation has been performed to study the dynamic switching behavior of the magnetization of the SAF free layer with tunable Ruderman–Kittel–Kasuya–Yosida interaction under the impact of an E-field.

Index Terms— Magnetic tunneling junction (MTJ), nonvolatile memory, Ruderman–Kittel–Kasuya–Yosida (RKKY), spin-transfer torque (STT), synthetic anti-ferromagnetic (SAF).

I. INTRODUCTION

MAGNETIC random-access memory (MRAM), a non-volatile memory using spins as storage bits, has earned interest in spintronic research as well as industry application since 1960s [2]–[7]. Except for the old writing process using local magnetic field [8], writing by spin-transfer torque (STT) [9], [10] and soon-came STT-MRAM [9]–[16] has caught people's attention for its great potential in non-volatility, scalability, high-speed operation, unlimited read/ write endurance, low energy consumption, and compatibility [8], [12], [16]–[25]. Different mechanisms such as spin Hall effect [26] and voltage controlled magnetic anisotropy [27], [28] have been proposed for new STT-MRAM development. However, the high switching current is still a critical issue as the huge Joule heat may destroy the stability of the storage elements—magnetic tunneling junctions (MTJs), and the storage will be no longer in force. To solve this problem, an electric-field (E-field)-assisted magnetization switching has been carried out since it could drastically lower the switching current than using pure STT for writing and reducing the size of access transistors, resulting in the higher bit density [29]. Besides, recent studies focusing on the E-field regulation of anti-ferromagnetism have gained increasing attention as well considering anti-ferromagnetic (AFM) materials are insensitive to magnetic field disturbance [30]. Nevertheless, the magnetic order in AFM materials is hard to tune for applicable use—since the alternative spins at the AFM/ferromagnetic (FM) interface are strongly pinned by AFM layer, these E-field control processes are usually confined at a low temperature [31], [32] or require a

magnetic-field assistance [33]. To overcome these difficulties, Yang *et al.* [1] studied the room temperature Ruderman–Kittel–Kasuya–Yosida (RKKY) interaction in the synthetic anti-ferromagnetic (SAF) multilayers only under the impact of E-field as a practical way to manipulate the RKKY interaction therein. This finding suggests that this E-field-controlled SAF multilayer can be utilized as a free layer (FL) in a traditional MTJ [34], [35]. Here, we propose a novel SAF-FL-MRAM design using E-field to modulate the RKKY interaction within the SAF-FL, which can reduce the critical switching current and then have great potential in enhancing bit density and depressing energy consumption.

II. MICROMAGNETIC SIMULATION

As shown in Fig. 1(a), the novel SAF-FL-MRAM design is consisted of the SAF-FL as well as a SAF pinned layer (SAF-PL) and a spacer layer (SL). The SL between PL and the bottom layer of SAF-FL is usually an insulator (e.g., MgO) for an MTJ, while the nonmagnetic (NM) layer between the bottom and top layers of the SAF-FL is usually a conductor; and in addition, the magnetization of the SAF-PL is fixed with its magnetization perpendicular to the plane. However, as the SAF-PL is used to generate spin-polarized current to switch the magnetization of FL by STT in the writing process and the SL is only important when reading the data with tunneling magnetoresistance (TMR), we can remove the SAF-PL and SL from simulation for simplicity and use a spin-polarized current to study the writing feature of the SAF-FL. In detail, we use object-oriented micromagnetic framework [36] to simulate the spin dynamic process of the SAF-FL, which is an FM/NM/FM multilayer with tunable RKKY interaction [37]. By changing the sign of the RKKY interaction via a small external E-field, the FM/NM/FM multilayer can reproduce the behavior of transformation between AFM and FM coupling states. Thus, the FM/NM/FM multilayer can be treated as the SAF-FL we mentioned above, and switched by injecting spin-polarized current.
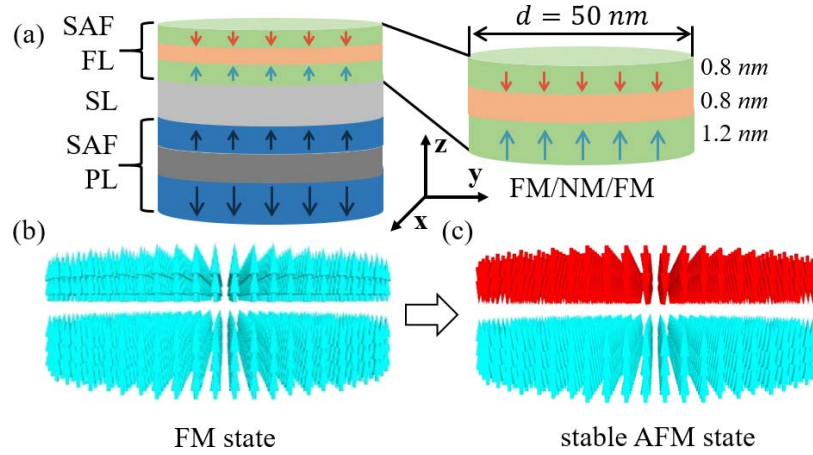
Fig. 1. Model of the MTJ. (a) Structure of the MTJ with SAF-PL/SL/SAF-FL and its zoomed-in view SAF-FL with diameter $d = 50$ nm and thicknesses $t_{\text{bott}} = 1.2$ nm, $t_{\text{NM}} = 0.8$ nm, and $t_{\text{top}} = 0.8$ nm for the bottom FM layer, NM layer, and top FM layer, respectively. All the magnetizations are perpendicular to the interfaces. (b) Sketch model of the FM state of the SAF-FL as the initial magnetization state. (c) Stable AFM state after micromagnetic evolution with setting $\sigma < 0$, which corresponds to the ground state without applying E-field.

In principle, the SAF-FL can be chosen as $(Pt/Co)_2$/Ru/ $(Co/Pt)_2$ or CoFeB/Ru/CoFeB for perpendicular or in-plane magnetization, respectively [1]. However, to keep the generality of this paper, we did not focus on a defined material, but work on a simple model instead. Technically, for the model of SAF-FL [Fig. 1(a) (right)], we define its diameter $d = 50$ nm and thicknesses of the FM (bottom)/NM/FM (top) layers to be $t_{\text{bott}} = 1.2$ nm, $t_{\text{NM}} = 0.8$ nm, and $t_{\text{top}} = 0.8$ nm, respectively. The SAF-FL is discretized into a lattice of axes parallel rectangular cells, and the size of one cell is $2 \times 2 \times 0.4 \text{nm}^3$. All the spins are governed by the Landau–Lifshitz–Gilbert–Slonczewski [38]–[41] equation, which reads

$$\frac{d\boldsymbol{m_i}}{d\tau} = -|\gamma| \boldsymbol{m_i} \times \boldsymbol{H}_{\text{eff}} + \alpha \left(\boldsymbol{m_i} \times \frac{d\boldsymbol{m_i}}{d\tau} \right)$$
$$+ |\gamma| \beta \epsilon (\boldsymbol{m_i} \times \boldsymbol{m_p} \times \boldsymbol{m_i}) - |\gamma| \beta \epsilon' (\boldsymbol{m_i} \times \boldsymbol{m_p}) \quad (1)$$

where $\boldsymbol{m_i}$ is the direction of magnetization in cell i, τ is the evolving time, γ is the gyromagnetic ratio, and the effective field $\boldsymbol{H}_{\text{eff}} = -(\partial D_{\text{tot}}/\partial \boldsymbol{M})$, (where D_{tot} is the total energy density of the SAF-FL, $\boldsymbol{M}$ is the magnetization). Typically, we chose FM = CoFeB as it is popular in the industry, and then the damping constant $\alpha = 0.01$ [42], [43] and the saturation magnetization $M_s = 1260$ emu/cm^3 [44] are used for a normal approach. For the STT part $\beta = |(\hbar/e\mu_0)|(J/tM_s)$, where J is the injected charge current density flowing perpendicular to the MTJ plane (in $\pm z$-direction), t is the thickness of the layer cell i, and $\epsilon = (P\Lambda^2/(\Lambda^2 + 1) + (\Lambda^2 - 1)(\boldsymbol{m} \times \boldsymbol{m_p}))$ determines the in-plane STT induced by J with $\Lambda = 1$ is the anisotropy effect of STT. Here, we set the polarized direction $\boldsymbol{m_p} = (\mathbf{0\,0\,1})$ with polarization P, and $\Lambda = 1$ to remove the dependence of ϵ on $\boldsymbol{m} \times \boldsymbol{m_p}$, and we set the secondary STT term $\epsilon' = 0.015$ to lead the ratio of field-like STT to Slonczewski STT to be 0.1 [45].

Moreover, in the simulation, we introduced the energy terms like the commonly Heisenberg exchange energy, anisotropy energy, demagnetization energy, and the RKKY interaction energy discussed above, which can be written as

$$D_{\text{tot}} = D_{\text{Heis}} + D_{\text{IA}} + D_{\text{demag}} + D_{\text{RKKY}} \quad (2)$$

where the Heisenberg exchange energy $D_{\text{Heis}} = \sum_{j \in N_i}$ $A(\boldsymbol{m_i} \times (\boldsymbol{m_i} - \boldsymbol{m_j})/\Delta_{ij}^2)$ with N_i the set consisting of the six cells nearest to cell i, the exchange coefficient $A = 30$ pJ/m [46], the discretization step size Δ_{ij} between cell i and cell j, and the interfacial perpendicular anisotropy energy $D_{\text{IA}} = D_{\text{IA}}^{\text{top}} + D_{\text{IA}}^{\text{bott}} = (K_I^{\text{top}}/t_{\text{top}})(1 - \boldsymbol{m_i} \times \boldsymbol{u})^2 + (K_I^{\text{bott}}/t_{\text{bott}})(1 - \boldsymbol{m_i} \times \boldsymbol{u})^2$ with $D_{\text{IA}}^{\text{top(bott)}}$ is the interface perpendicular anisotropy energy of the top (bottom) layer of the SAF-FL, $K_I^{\text{top(bott)}}$ is the corresponding interface perpendicular anisotropy energy density, $\boldsymbol{u}$ is the interface perpendicular anisotropy direction, which is set to be along $(\mathbf{0\,0\,1})$ in this paper and the demagnetization energy D_{demag} is also included automatically.

One may notice that the two FM layers are very thin so that the perpendicular anisotropy is dominated by the two surfaces, i.e., the interface between the bottom layer of SAF-FL and its adjacent SL, and the interface between the top FM layer of SAF-FL and its adjacent capping layer (not shown) that is why we set the bulk magnetic anisotropy $K_B^{\text{top}} = K_B^{\text{bott}} = 0$ and only take into account the interface perpendicular anisotropy [26], which we use $K_I^{\text{top}} = 0.96$ erg/cm^2 and $K_I^{\text{bott}} = 1.44$ erg/cm^2 in this paper. To further test the thermal stability of the SAF-FL which is much important for applications, we calculated the thermal stability factor $\Delta = E_A/(k_B T)$, where

$$E_A = \left(-\frac{\mu_0 M_S^2}{2} + K_B^{\text{top}} + \frac{K_I^{\text{top}}}{t_{\text{top}}} \right) V_{\text{top}}$$
$$+ \left(-\frac{\mu_0 M_S^2}{2} + K_B^{\text{bott}} + \frac{K_I^{\text{bott}}}{t_{\text{bott}}} \right) V_{\text{bott}} \quad (3)$$

is the energy barrier [26] that separates the two magnetization states of the SAF-FL, and $V_{\text{top(bott)}}$ is the volume of the top (bottom) layer of SAF-FL, k_B is Boltzmann's constant, T is the temperature, and $-\mu_0 M_S^2/2$ is the distribution of demagnetization. Then, we get $\Delta = 199$ using $T = 300$ K, which denotes very good thermal stability as that a more than 10 years retention of the data [47].

The additional RKKY interaction energy is the key issue of this paper, which is included by introducing an extra energy (density) term as

$$D_{\text{RKKY}} = \frac{\sigma[1 - \boldsymbol{m}_k \times \boldsymbol{m}_l] + \sigma_2[1 - (\boldsymbol{m}_k \times \boldsymbol{m}_l)^2]}{\delta_{kl}} \quad (4)$$

where σ and σ_2, respectively, are the bilinear and biquadratic surface exchange coefficients (RKKY) between the two FM layers of SAF-FL, and here we keep $\sigma_2 = 0$ all the time for simple. $\boldsymbol{m}_k$ and $\boldsymbol{m}_l$ are the magnetization directions at cell k and cell l which belong to different FM layers, δ_{kl} is the discretization step size in the direction from cell k toward cell l. One should notice that if σ is negative, then the ground state of the SAF-FL will be AFM due to the RKKY interaction energy will reach minimum when the two FM layers are anti-parallel.

There are generally two ways to modulate the RKKY interaction within the SAF-FL: i) by changing the thickness of the NM layer, the two FM layers can be AFM coupled or FM coupled [48] and ii) by applying an *E*-field efficiently as found recently [1]. However, as the size of a device cannot be changed after MTJ is deposited, the *E*-field becomes a convenient way to realize controllable RKKY interaction for SAF-FL. Here, we use the micromagnetic modeling to simulate the *E*-field-assisted magnetization switching behavior of the SAF-FL with tunable RKKY interaction.

In the SAF-FL, the magnetizations of its bottom and top layers can be parallel if the RKKY interaction favors an FM state (positive σ) or anti-parallel if the RKKY interaction favors an AFM state (negative σ). As shown in Fig. 1(b), we initially set the magnetization state ($\boldsymbol{m}_0$) of the SAF-FL to be parallel before the calculations, and start the simulation with setting $\sigma < 0$, and finally obtain a stable AFM state of SAF-FL after micromagnetic evolution, as shown in Fig. 1(c), which confirm our understanding on the RKKY interaction energy term. This AFM state will be treated as an initialized ground state of SAF-FL. Moreover, we can see that the magnetization of the thinner top layer changes its orientation to be anti-parallel to the magnetization of the thicker bottom layer. This is because the anisotropy energy of the bottom layer ($E_I^{\text{bott}} = K_I^{\text{bott}} \times \pi d^2/4$) is set to be 50% higher than that of the top layer ($E_I^{\text{top}} = K_I^{\text{top}} \times \pi d^2/4$) so that the top layer can more easily switch its magnetization while the magnetization of the bottom layer keeps its orientation to form an AFM state. This feature of the SAF-FL is very important for storage, as the total resistance of the MTJ in Fig. 1(a) comes from two parts: TMR of "top layer of SAF-PL/SL/bottom layer of SAF-FL" stacked structure and giant magnetoresistance (GMR) of SAF-FL itself; however, the resistance of the MTJ is dominated by TMR, due to TMR is much larger than GMR. So, we need to keep the bottom layer of SAF-FL unchanged after the external *E*-field is rescinded to make sure that we do not need to keep the *E*-field after writing.

III. RESULTS

Within the above frame, we set the AFM state of SAF-FL in Fig. 1(c) as the initial magnetization state in the
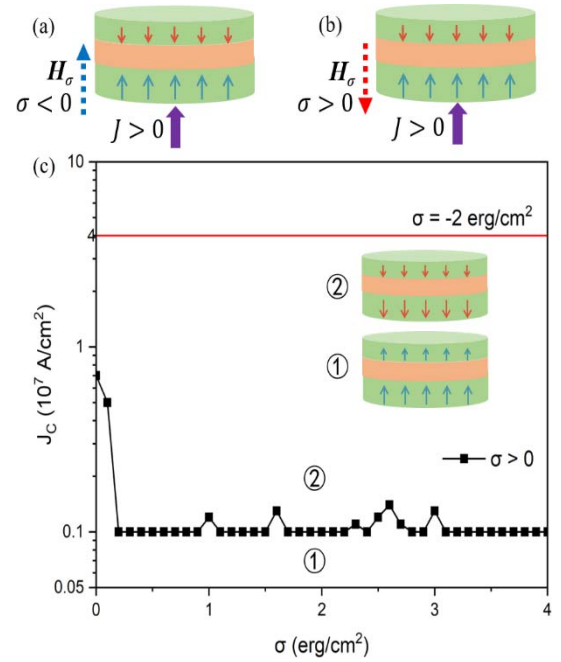

Fig. 2. *E*-field-assisted magnetization switching by charge current-induced STT. (a) and (b) Model of the effective magnetic field induced by RKKY interaction with $\sigma < 0$ and $\sigma > 0$, respectively. $\boldsymbol{H}_\sigma$ stands for the direction of this effective magnetic field. (c) Critical switching current density J_C as a function of σ, and here we also plot the critical switching current density with $\sigma = -2$ erg/cm^2 for comparison. All the initial magnetization state of SAF-FL is an AFM state as shown in Fig. 1(c). ① and ② are the sketch models for the magnetization configuration before and after switching. Clearly, we can see that, for $\sigma \geq 0.2$ erg/cm^2, J_{SW} can be as low as 0.1 or 0.2×10^7 A/cm^2, which is one magnitude smaller than that $J_C = 4 \times 10^7$ A/cm^2 with $\sigma = -2$ erg/cm^2.

following simulations. The switching process of the magnetization of the bottom layer of the SAF-FL has been studied using charge current J under the assisting *E*-field. As we discussed previously, when without applied *E*-field, the RKKY interaction favors an AFM state; therefore, the bottom layer feels an effective magnetic field $\boldsymbol{H}_\sigma$ pointing oppositely to the magnetization of the top layer as shown in Fig. 2(a) due to the RKKY will force the magnetization of the bottom layer to be anti-parallel to the magnetization of the top layer, and this $\boldsymbol{H}_\sigma$ will help to pin the magnetization of the bottom layer, which will make it much harder to be switched by charge current J than normal FM FL case. But when *E*-field is applied, the RKKY interaction favors an FM state, in this case, $\boldsymbol{H}_\sigma$ points in the same direction with the magnetization of the top layer as shown in Fig. 2(b), which can assist the STT of J to switch the magnetization of the bottom layer and end up with a much smaller critical switching current density J_C. Numerically, J_C for switching the magnetization of the bottom layer of SAF-FL can be obtained as a function of RKKY interaction, as shown in Fig. 2(c), from which we can conclude that, compared with $J_C = 4 \times 10^7$ A/cm^2 with a negative RKKY interaction ($\sigma = -2$ erg/cm^2), the switching process only needs a weak charge current density which is even smaller than 0.2×10^7 A/cm^2 (20 times reduction) when the RKKY tuned by the *E*-field to a positive value $\sigma \geq 0.2$ erg/cm^2. In this sense, the energy reduction during writing process using *E*-field-assisted magnetization switching can be at least 2 orders of magnitude smaller than
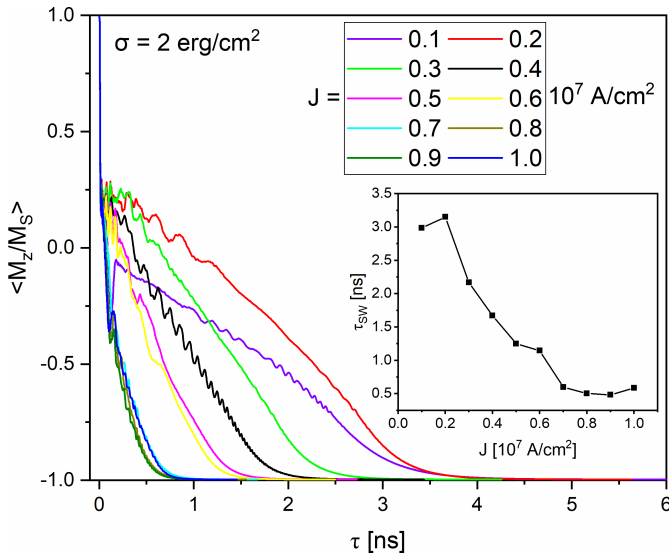
Fig. 3. Averaged magnetization $\langle M_z/M_S \rangle$ of the bottom layer as a function of evolving time τ with $\sigma = 2$ erg/cm^2 and varying charge current density J, the initial magnetization state of SAF-FL is an AFM state as in Fig. 1(c). Inset: switching time τ_{SW} as a function of J. Here, we define that the magnetization switching of the bottom layer is completed when $\langle M_z/M_S \rangle$ is smaller than -0.9.

Fig. 4. Averaged magnetization $\langle M_z/M_S \rangle$ of the bottom layer as a function of evolving time τ with $J = 0.4 \times 10^7$ A/cm^2 and varying σ, the initial magnetization state of SAF-FL is an AFM state as in Fig. 1(c). Inset: switching time τ_{SW} as a function of σ with the same definition in Fig. 3

that without applying E-field, according to the simple Joule's law estimation $Q = I^2 Rt$, which makes this E-field-controlled SAF-FL-MRAM design much more advantageous than today's STT-MRAM.

Note that unfortunately we have not found a clear relation between σ (RKKY) and E-field yet, and what we know is that this relation is strongly dependent on the details of the SAF-FL [1]. However, as shown in Fig. 2(c), the reduction of J_C is not sensitive to σ, which means that we only need the E-field-controlled AFM–FM transition to make our design works.

The fast switching time is critical for the STT-MRAM as the static random-access memory (SRAM) replacement candidate, especially in the sub-5 ns region [49]. So, we then go deep into the relationships between the switching time of the magnetization of the bottom layer of SAF-FL and the charge current density as well as the strength of the RKKY interaction. Fig. 3 shows the averaged magnetization $\langle M_z/M_S \rangle$ of the bottom layer as a function of evolving time τ with $\sigma = 2$ erg/cm^2 and varying charge current density J from 0.1 to 1×10^7 A/cm^2. We can see that generally the time used for $\langle M_z/M_S \rangle$ changing from 1 to -1 decrease along with J increases from 0.1 to 0.7×10^7 A/cm^2. Here, we can define that the magnetization switching of the bottom layer is completed when $\langle M_z/M_S \rangle$ is smaller than -0.9, then the critical switching time can be obtained as plotted in the inset of Fig. 3, which gives the switching time τ_{SW} as a function of J. One may have noticed that the magnetization evolution shows a peculiar transient in Fig. 3 at the beginning. This is because we add the E-field at the same time as the charge current is applied. So, at the very beginning, the SAF-FL changes from AFM state to FM state suddenly, which makes the magnetization change very fast even before the charge current gives any contribution. Also, Fig. 4 shows $\langle M_z/M_S \rangle$ of the bottom layer as a function of evolution time τ with
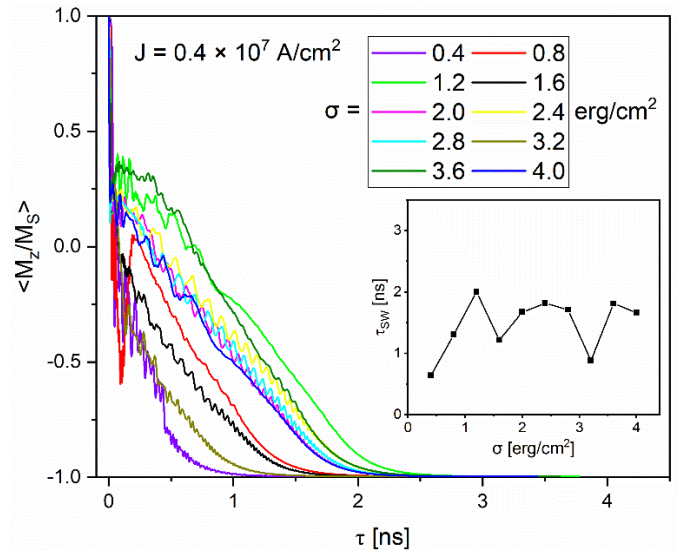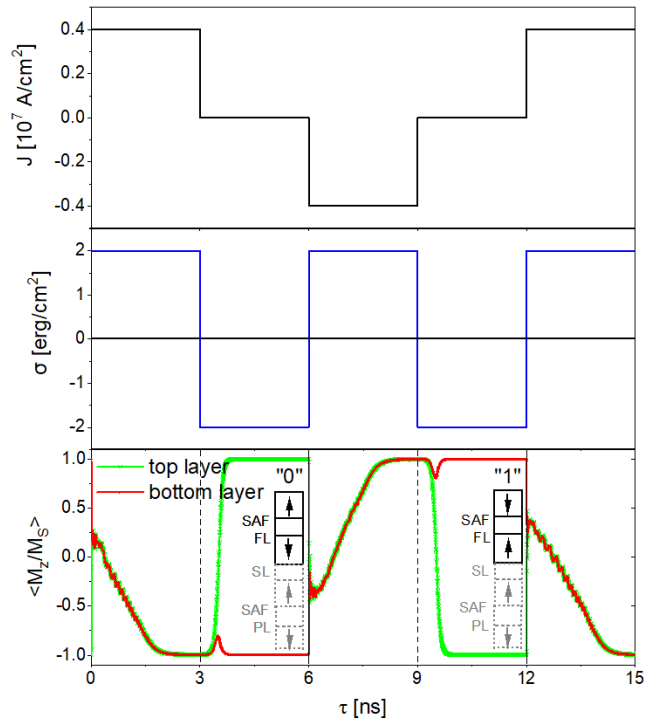

Fig. 5. Writing process for a typical SAF-FL-MRAM device. (a) and (b) Applied time-dependent charge current density J and E-field (the value of σ instead), respectively. Here, we chose a 3 ns writing pulse and then the period is 12 ns. (c) Averaged magnetization $\langle M_z/M_S \rangle$ of the top and bottom layers as a function of evolving time τ. Here, we define the magnetization state of MTJ during $\tau = 36$ ns to be binary 0, and the magnetization state of MTJ during $\tau = 912$ ns to be binary 1, the two sketches of binary 0 and binary 1 are inserted at $\tau = 36$ ns and $\tau = 912$ ns, respectively.

$J = 0.4 \times 10^7$ A/cm^2 and varying σ from 0.4 to 4 erg/cm^2, and with the same definition as that in the inset of Fig. 3, τ_{SW} as a function of σ are plotted in the inset of Fig. 4, differently the switching times are all under about 2 ns for $J = 0.4 \times 10^7$ A/cm^2, which demonstrates that the switching time is insensitive to the E-field strength. Based on this,
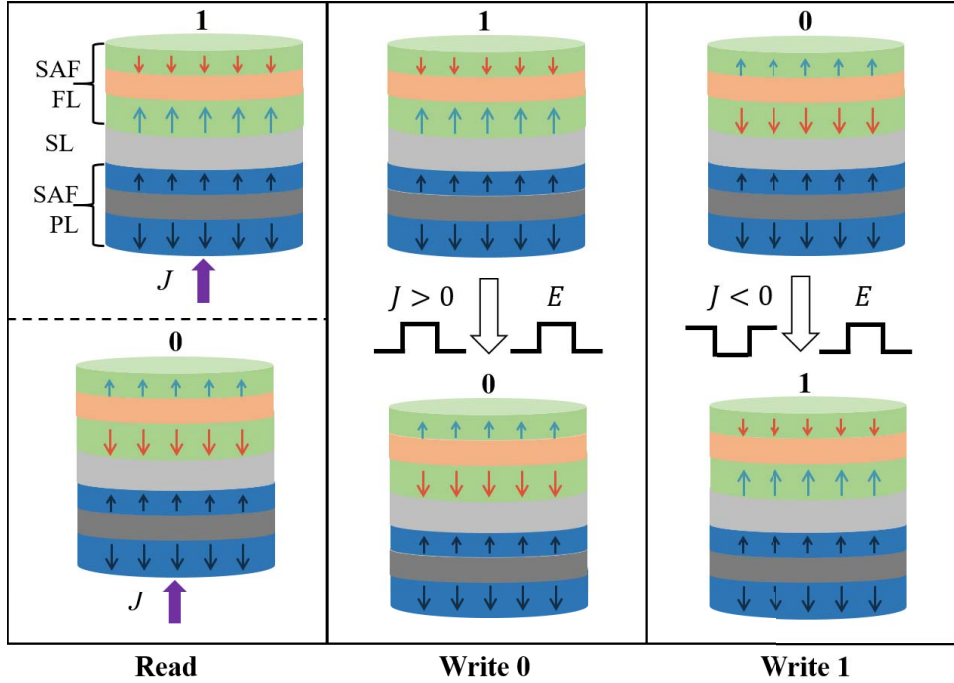
Fig. 6. MTJ as a storage element of the SAF-FL-MRAM and its read/write mechanisms. (a) Reading process with small charge current and the magnetoresistance from TMR. (b) and (c) Writing process this positive or negative charge current pulse for write binary 0 and binary 1, respectively.

we can set a robust parameter for writing with a 3 ns pulse with $\sigma = 2$ erg/cm^2 which results in a critical switching current density less than $J = 0.4 \times 10^7$ A/cm^2, and this will results in a 3 ns STT-MRAM, which is already potentially good enough for level-2 cache SRAM replacement.

Moreover, we apply 3 ns charge current pulses and *E*-field pulses (the value of σ instead) as shown in Fig. 5(a) and (b), respectively, to show how to write binary 0 and binary 1. For the first 3 ns, a positive charge current $J = 0.4 \times 10^7$ A/cm^2 and an *E*-field ($\sigma = 2$ erg/cm^2) are applied, then at $\tau = 3 \sim 6$ ns, charge current and *E*-field are removed ($J = 0$ and $\sigma = -2$ erg/cm^2), at $\tau = 6 \sim 9$ ns, a negative charge current (density) $J = -0.4 \times 10^7$ A/cm^2 and an *E*-field ($\sigma = 2$ erg/cm^2) are applied, at $\tau = 9 \sim 12$ ns, and charge current and *E*-field are again removed ($J = 0$ and $\sigma = -2$ erg/cm^2). The last $12 \sim 15$ ns is the first quarter part of a new time cycle. Fig. 5(c) shows $\langle M_z/M_S \rangle$ of the top and bottom layers as a function of τ. We can see that at $\tau = 0 \sim 3$ ns, $\langle M_z/M_S \rangle$ of the bottom layer successfully changes from 1 to -1, and $\langle M_z/M_S \rangle$ of the top layer has a large disturbance, but finally returns to -1; then at $\tau = 3 \sim 6$ ns, $\langle M_z/M_S \rangle$ of the bottom layer stays at -1 after a small disturbance, while $\langle M_z/M_S \rangle$ of the top layer changes from -1 to 1; for $\tau = 6 \sim 9$ ns and $\tau = 9 \sim 12$ ns, $\langle M_z/M_S \rangle$ of the bottom and the top layers show a similar manner as the first writing process; at $\tau = 12 \sim 15$ ns, the magnetizations of the bottom and top layers evolve just as that in $\tau = 0 \sim 3$ ns, which mean another period appears. Here, we can define the magnetization state of MTJ during $\tau = 3 \sim 6$ ns to be binary 0, and the magnetization state of MTJ during $\tau = 9 \sim 12$ ns to be binary 1, the two sketches of binary 0 and binary 1 are inserted at $\tau = 3 \sim 6$ ns and $\tau = 9 \sim 12$ ns, respectively.

In the end, we show the read/write mechanisms in the SAF-FL-MRAM device in Fig. 6. As shown in the top and bottom panels of Fig. 6(a), by applying a small charge current through the whole MTJ with no matter the J flows from SAF-PL to SAF-FL or reverse, the total magnetoresistance which is governed by TMR from "top layer of SAF-PL/SL/ bottom layer of SAF-FL" stacked structure can be measured and therefore read its binary state 1 or 0. For writing, as shown in Fig. 6(b) and (c), by applying a positive or negative charge current pulses and an *E*-field pulse at the same time, we can write MTJ from binary 1 to binary 0 or from binary 0 to binary 1. One should notice that in a real system, the charge current is applied using two normal leads as what we are usually using in MTJs to generate STT. For the *E*-field, an ionic liquid gating technic [1] can be used, and as it does not build up a closed circuit inside the SAF-FL, it will not affect the applied charge current. Moreover, as the electric current and *E*-field are generated by two sets of transistors, the charge current and *E*-field can be controlled individually.

IV. Conclusion

With micromagnetic simulation, a new SAF-FL-MRAM has been proposed, and with the tunable RKKY interaction in the SAF-FL of MTJ, the switching current can be reduced by 20 times which ends up with almost 2 order of magnitude smaller energy dissipation. In detail, the writing speed can be fast enough as 3 ns with switching current less than $J = 4 \times 10^6$ A/cm^2, which is potentially good enough for level-2 cache SRAM replacement. As the data are stored with an SAF-FL with strong AFM coupling, which make it is less sensitive to external magnetic field disturbance.

REFERENCES

[1] Q. Yang *et al.*, "Ionic liquid gating control of RKKY interaction in FeCoB/Ru/FeCoB and (Pt/Co)$_2$/Ru/(Co/Pt)$_2$ multilayers," *Nature Commun.*, vol. 9, no. 1, p. 991, 2018.

[2] S. Bhatti, R. Sbiaa, A. Hirohata, H. Ohno, S. Fukami, and S. N. Piramanayagam, "Spintronics based random access memory: A review," *Mater. Today*, vol. 20, no. 9, pp. 530–548, 2017.

[3] J. I. Raffel and T. S. Crowther, "A proposal for an associative memory using magnetic films," *IEEE Trans. Electron. Comput.*, vol. EC-13, no. 5, p. 611, 1964.

[4] M. N. Baibich *et al.*, "Giant magnetoresistance of (001)Fe/(001)Cr magnetic superlattices," *Phys. Rev. Lett.*, vol. 61, no. 21, pp. 2472–2475, 1988.

[5] G. Binasch, P. Grünberg, F. Saurenbach, and W. Zinn, "Enhanced magnetoresistance in layered magnetic structures with antiferromagnetic interlayer exchange," *Phys. Rev. B, Condens. Matter*, vol. 39, no. 7, pp. 4828–4830, 1989.

[6] T. Miyazaki and N. Tezuka, "Giant magnetic tunneling effect in Fe/Al$_2$O$_3$/Fe junction," *J. Magn. Magn. Mater.*, vol. 139, no. 3, pp. L231–L234, 1995.

[7] J. S. Moodera, L. R. Kinder, T. M. Wong, and R. Meservey, "Large magnetoresistance at room temperature in ferromagnetic thin film tunnel junctions," *Phys. Rev. Lett.*, vol. 74, no. 16, pp. 3273–3276, Apr. 1995.

[8] B. N. Engel *et al.*, "A 4-Mb toggle MRAM based on a novel bit and switching method," *IEEE Trans. Magn.*, vol. 41, no. 1, pp. 132–136, Jan. 2005.

[9] J. C. Slonczewski, "Current-driven excitation of magnetic multilayers," *J. Magn. Magn. Mater.*, vol. 159, no. 1, pp. L1–L7, 1996.

[10] L. Berger "Emission of spin waves by a magnetic multilayer traversed by a current," *Phys. Rev. B, Condens. Matter*, vol. 54, no. 13, p. 9353, 1996.

[11] J. A. Katine, F. J. Albert, R. A. Buhrman, E. B. Myers, and D. C. Ralph, "Current-driven magnetization reversal and spin-wave excitations in Co/Cu/Co pillars," *Phys. Rev. Lett.*, vol. 84, no. 14, pp. 3149–3152, 2000.

[12] W. Kim *et al.*, "Extended scalability of perpendicular STT-MRAM towards sub-20 nm MTJ node," in *IEDM Tech. Dig.*, Dec. 2011, pp. 531–534.

[13] M. Gajek *et al.*, "Spin torque switching of 20 nm magnetic tunnel junctions with perpendicular anisotropy," *Appl. Phys. Lett.*, vol. 100, no. 13, p. 132408, 2012.

[14] T. Kawahara, K. Ito, R. Takemura, and H. Ohno, "Spin-transfer torque RAM technology: Review and prospect," *Microelectron. Rel.*, vol. 52, no. 4, pp. 613–627, Apr. 2012.

[15] A. V. Khvalkovskiy *et al.*, "Basic principles of STT-MRAM cell operation in memory arrays," *J. Phys. D, Appl. Phys.*, vol. 46, no. 7, p. 74001, Jan. 2013.

[16] Q. J. Yap *et al.*, "Phase ordering and its effect on magnetic and structural properties of FeRh ultrathin films," *J. Appl. Phys.*, vol. 116, no. 4, p. 043902, 2014.

[17] S. Tehrani, "Status and outlook of MRAM memory technology (invited)," in *IEDM Tech. Dig.*, Dec. 2006, pp. 1–4.

[18] J. M. Slaughter *et al.*, "High density ST-MRAM technology (invited)," in *IEDM Tech. Dig.*, Dec. 2012, pp. 29.3.1–29.3.4.

[19] S. Yuasa *et al.*, "Future prospects of MRAM technologies," in *IEDM Tech. Dig.*, Dec. 2013, pp. 3.1.1–3.1.4.

[20] M. Durlam *et al.*, "A 0.18 μm 4 Mb toggling MRAM," in *Proc. Int. Conf. Integr. Circuit Design Technol.*, May 2003, pp. 27–30.

[21] T. Min *et al.*, "Interconnects scaling challenge for sub-20nm spin torque transfer magnetic random access memory technology," in *Proc. IEEE Int. Interconnect Technol. Conf.*, May 2014, pp. 341–344.

[22] T. Min *et al.*, "A study of write margin of spin torque transfer magnetic random access memory technology," *IEEE Trans. Magn.*, vol. 46, no. 6, pp. 2322–2327, Jun. 2010.

[23] J.-G. Zhu, "Method of writing data with binary anisotropy media," U.S. Patent 8 675 456 B2, Mar. 18, 2014.

[24] J.-G. Zhu, "Apparatus for removing printed sheets for inspection," U.S. Patent 0 180 827 A1, Mar. 7, 1988.

[25] J.-G. Zhu, "Laser beam diverter and robotic assembly comprising a laser beam diverter," U.S. Patent 0 237 987 A1, Nov. 13, 1991.

[26] A. van den Brink, "Spin-Hall-assisted magnetic random access memory," *Appl. Phys. Lett.*, vol. 104, no. 1, pp. 12401–12404, 2014.

[27] P. Khalili and K. Wang, "Electric-field-controlled MRAM based on voltage control of magnetic anisotropy (VCMA): Recent progress and perspectives," in *Proc. 4th Berkeley Symp. Energy Efficient Electron. Syst. (E3S)*, 2015, p. 1.

[28] PK Amiri, KL Wang, K Galatsis, "Voltage-controlled magnetic anisotropy (VCMA) switch and magneto-electric memory (MeRAM)," U.S. Patent 9 129 691, Sep. 8, 2015.

[29] C. Grezes *et al.*, "Ultra-low switching energy and scaling in electric-field-controlled nanoscale magnetic tunnel junctions with high resistance-area product," *Appl. Phys. Lett.*, vol. 108, no. 1, p. 012403, 2016.

[30] T. Jungwirth, X. Marti, P. Wadley, and J. Wunderlich, "Antiferromagnetic spintronics," *Nature Nanotechnol.*, vol. 11, no. 3, pp. 231–241, 2016.

[31] Y. Wang *et al.*, "Electrical control of the exchange spring in antiferromagnetic metals," *Adv. Mater.*, vol. 27, no. 20, pp. 3196–3201, 2015.

[32] V. Laukhin *et al.*, "Electric-field control of exchange bias in multiferroic epitaxial heterostructures," *Phys. Rev. Lett.*, vol. 97, no. 22, pp. 1–4, 2006.

[33] M. Liu, J. Lou, S. Li, and N. X. Sun, "E-field control of exchange bias and deterministic magnetization switching in AFM/FM/FE multiferroic heterostructures," *Adv. Funct. Mater.*, vol. 21, no. 3, pp. 2593–2598, 2011.

[34] S. Bandiera *et al.*, "Comparison of synthetic antiferromagnets and hard ferromagnets as reference layer in magnetic tunnel junctions with perpendicular magnetic anisotropy," *IEEE Magn. Lett.*, vol. 1, 2010, Art. no. 3000204.

[35] C. Augustine, A. Raychowdhury, D. Somasekhar, J. Tschanz, K. Roy, and V. K. De, "Numerical analysis of typical STT-MTJ stacks for 1T-1R memory arrays," in *IEDM Tech. Dig.*, Dec. 2010, pp. 22.7.1–22.7.4.

[36] M. J. Donahue and D. G. Porter, "OOMMF user's guide, version 1.0," Nat. Inst. Standards Technol., Gaithersburg, MD, USA, Tech. Rep. 6376, Sep. 1999.

[37] M. A. Ruderman and C. Kittel, "Indirect exchange coupling of nuclear magnetic moments by conduction electrons," *Phys. Rev.*, vol. 96, no. 1, pp. 99–102, 1954.

[38] A. V. Khvalkovskiy *et al.*, "High domain wall velocities due to spin currents perpendicular to the plane," *Phys. Rev. Lett.*, vol. 102, no. 6, p. 067206, 2009.

[39] T. L. Gilbert, "A Lagrangian formulation of the gyromagnetic equation of the magnetization field," *Phys. Rev.*, vol. 100, p. 1243, 1955.

[40] L. Landau and E. Lifshits, "On the theory of the dispersion of magnetic permeability in ferromagnetic bodies," *Phys. Zeitsch. Sow.*, vol. 169, no. 14, pp. 14–22, 1935.

[41] J. Xiao, A. Zangwill, and M. D. Stiles, "Boltzmann test of Slonczewski's theory of spin-transfer torque," *Phys. Rev. B, Condens. Matter*, vol. 70, no. 17, pp. 1–4, 2004.

[42] X. Liu, W. Zhang, M. J. Carter, and G. Xiao, "Ferromagnetic resonance and damping properties of CoFeB thin films as free layers in MgO-based magnetic tunnel junctions," *J. Appl. Phys.*, vol. 110, no. 3, p. 033910, 2011.

[43] T. Devolder, "Damping of Co$_x$Fe$_{80-x}$B$_{20}$ ultrathin films with perpendicular magnetic anisotropy," *Appl. Phys. Lett.*, vol. 102, no. 2, p. 022407, 2013.

[44] S. Ikeda *et al.*, "A perpendicular-anisotropy CoFeB-MgO magnetic tunnel junction," *Nature Mater.*, vol. 9, no. 9, pp. 721–724, Jul. 2010.

[45] S. Zhang *et al.*, "Current-induced magnetic skyrmions oscillator," *New J. Phys.*, vol. 17, p. 023061, Feb. 2015.

[46] D. V. Berkov, C. T. Boone, and I. N. Krivorotov, "Micromagnetic simulations of magnetization dynamics in a nanowire induced by a spin-polarized current injected via a point contact," *Phys. Rev. B, Condens. Matter*, vol. 83, no. 5, pp. 1–10, 2011.

[47] S. Ikeda *et al.*, "Magnetic tunnel junctions for spintronic memories and beyond," *IEEE Trans. Electron Devices*, vol. 54, no. 5, pp. 991–1002, May 2007.

[48] S. S. P. Parkin and D. Mauri, "Spin engineering: Direct determination of the Ruderman-Kittel-Kasuya-Yosida far-field range function in ruthenium," *Phys. Rev. B, Condens. Matter*, vol. 44, no. 13, pp. 7131–7134, 1991.

[49] J. Guenole *et al.*, "Achieving Sub-ns switching of STT-MRAM for future embedded LLC applications through improvement of nucleation and propagation switching mechanisms," in *Symp. VLSI Technol. Dig. Tech. Paper*, Sep. 2015, pp. 50–51.